UCRL-JC-125226
PREPRINT

Proximity Effect and Hot-Electron Diffusion in $Ag/Al_2O_3/Al$ Tunnel Junctions

H. Netel, J. Jochum, S. E. Labov, C. A. Mears, M. Frank,
D. Chow, M. A. Lindeman, L. J. Hiller

This paper was prepared for submittal to the
1996 Applied Superconductivity Conference
Pittsburgh, PA
August 25-30, 1996

February 18, 1997

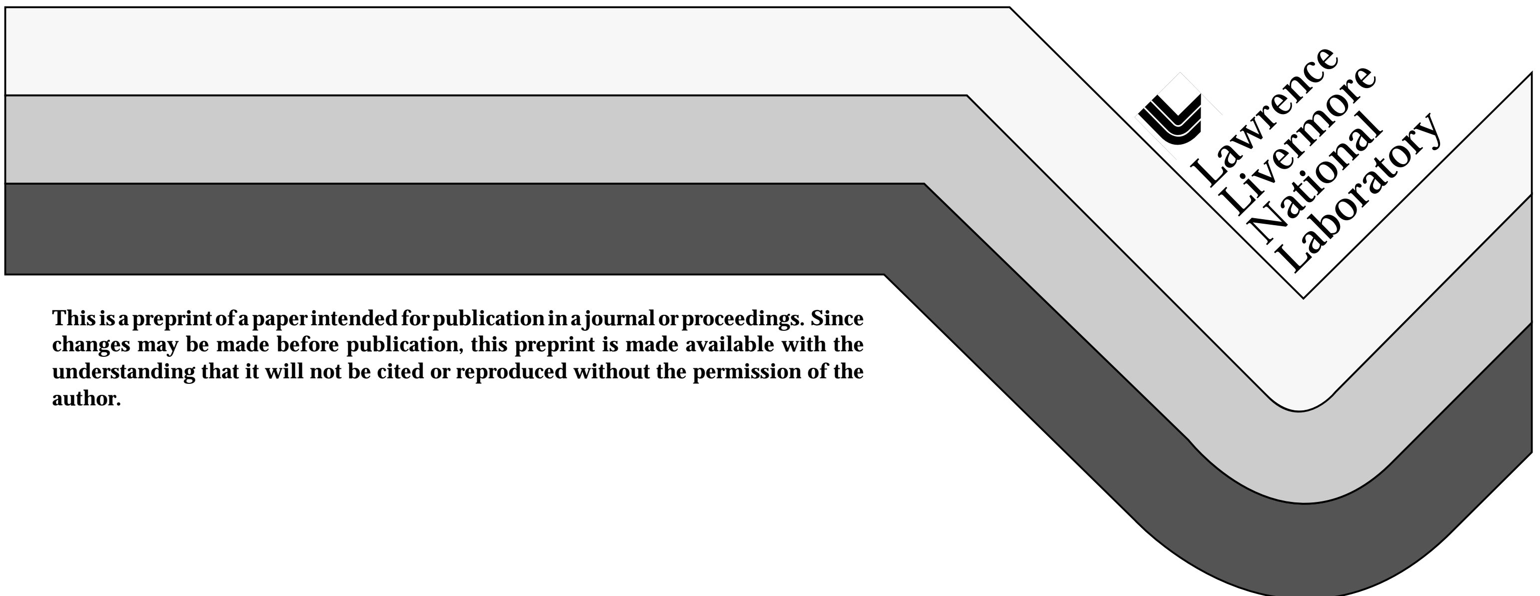

This is a preprint of a paper intended for publication in a journal or proceedings. Since changes may be made before publication, this preprint is made available with the understanding that it will not be cited or reproduced without the permission of the author.

DISCLAIMER

This document was prepared as an account of work sponsored by an agency of the United States Government. Neither the United States Government nor the University of California nor any of their employees, makes any warranty, express or implied, or assumes any legal liability or responsibility for the accuracy, completeness, or usefulness of any information, apparatus, product, or process disclosed, or represents that its use would not infringe privately owned rights. Reference herein to any specific commercial product, process, or service by trade name, trademark, manufacturer, or otherwise, does not necessarily constitute or imply its endorsement, recommendation, or favoring by the United States Government or the University of California. The views and opinions of authors expressed herein do not necessarily state or reflect those of the United States Government or the University of California, and shall not be used for advertising or product endorsement purposes.

Proximity Effect and Hot-Electron Diffusion in $Ag/Al_2O_3/Al$ Tunnel Junctions

H. Netel, J. Jochum, Simon E. Labov, C. A. Mears and M. Frank
Physics and Space Technology Directorate, Lawrence Livermore National Laboratory, PO Box 808, L-401, Livermore, CA 94550

D. Chow, M. A. Lindeman and L. J. Hiller
Department of Applied Science, University of California at Davis, PO Box 808, L-401, Livermore, CA 94550

Abstract **— We have fabricated $Ag/Al_2O_3/Al$ tunnel junctions on Si substrates using a new process. This process was developed to fabricate superconducting tunnel junctions (STJs) on the surface of a superconductor. These junctions allow us to study the proximity effect of a superconducting Al film on a normal metal trapping layer. In addition, these devices allow us to measure the hot-electron diffusion constant using a single junction. Lastly these devices will help us optimize the design and fabrication of tunnel junctions on the surface of high-Z, ultra-pure superconducting crystals.**

1. Introduction

We are developing a new generation of cryogenic X-ray detectors in which the energetic photons are absorbed in a high-Z, ultra-pure superconducting crystal [1]. When a photon is absorbed in the superconducting absorber it breaks up the Cooper pairs and produces a non-equilibrium distribution of quasiparticles and phonons. The number of quasiparticles produced is proportional to the energy of the absorbed photon. This number, and thus the energy of the absorbed photon, can be measured when the superconducting absorber is coupled to an appropriate sensor. This sensor can either be a superconductor - insulator - superconductor (SIS) tunnel junction, which measures an increase in the tunneling current [2], or a normal metal - insulator - superconductor (NIS) tunnel junction, which measures a temperature rise of the normal metal electrode [3].

In our first generation of devices [1] we created an insulating layer on the surface of a Ta crystal by means of anodic oxidation. It was found that the $Al/Al_2O_3/Al$ tunnel junctions on top of these layers showed I-V characteristics with small superconducting shorts in parallel to the junction barriers. This was probably caused by an increased surface roughness of the anodized surface of the crystal. Atomic force microscopy measurements show an RMS surface roughness of 600 Å for the Ta_2O_5 as compared to 10 - 12 Å for the mechanically polished Ta. In order to avoid this problem we developed a new fabrication process in which the tunnel junctions can be deposited directly on the surface of the superconducting crystal. With this process we can fabricate both $Al/Al_2O_3/Al$ SIS as well as $Ag/Al_2O_3/Al$ NIS tunnel junctions. In order to optimize this new fabrication process, and to study the proximity effect of the superconducting crystal on the energy gap of the Al and Ag thin films, we fabricated devices on Si substrates with a thin Al film in place of the Ta crystal.

Manuscript received August 27, 1996.

This work was performed under the auspices of the U.S. Department of Energy by Lawrence Livermore National Laboratory under contract No. W-7405-ENG-48.

We acknowledge the funding of J. Jochum by the Alexander von Humboldt Foundation. This work was also partially funded by the Institute of Geophysics and Planetary Physics at Lawrence Livermore National Laboratory.

2. Device Fabrication

A schematic cross-section of one of our $Ag/Al_2O_3/Al$ NIS tunnel junctions is shown in Fig. 1. All the metal films are deposited by DC magnetron sputtering and structured using BeCu shadow masks. The first fabrication step is the deposition of a 200 nm thick Al base film. A 200 nm thick Ag base electrode is then deposited, followed by a 20 nm thick Al seed layer. The sample is oxidized in the load-lock for 30 minutes at an oxygen pressure of 1.0 Torr, after which the 200 nm thick Al counter electrode is deposited. The next step is the deposition of an insulating layer which electrically isolates the wiring layer from the base film and has small holes to allow contact to the counter electrodes of the

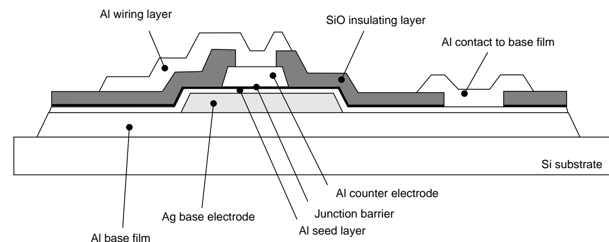

Fig. 1. Schematic cross-section of a $Ag/Al_2O_3/Al$ tunnel junction fabricated on a 200 nm thick Al base film on a Si substrate. The Ag base electrode has an area of 200 x 300 μm^2 and is 200 nm thick. The Al seed layer covers the whole Al base film and is 20 nm thick. The 200 nm thick Al counter electrode defines the area of the tunnel junction and has an area of 100 x 100 μm^2. Note that the Ag base electrode is much larger than the tunnel junction area.

junctions. A 700 nm thick thermally evaporated layer of SiO is deposited, and the holes are defined by means of lift-off. The last step is the deposition of the 500 nm thick Al wiring layer and the 200 nm thick Al film that makes contact to the Al base film.

3. RESULTS

We fabricated both $Ag/Al_2O_3/Al$ tunnel junctions and $Al/Al_2O_3/Al$ tunnel junctions with the process described in section 2. The $Al/Al_2O_3/Al$ devices were basically the same as the one shown in Fig. 1. The only difference is that the Ag base electrode and the Al seed layer are left out of the device. The devices were cooled in an adiabatic demagnetization refrigerator. We use the ratio R_D, the dynamic resistance in the subgap region, to R_N, the normal state resistance of the tunnel junction, to parametrize the junction quality. The $Al/Al_2O_3/Al$ devices showed typical SIS I-V characteristics with quality factors R_D/R_N up to $4.6 \cdot 10^5$.

The $Ag/Al_2O_3/Al$ tunnel junctions fabricated with this new process were also very good. We measured quality factors ranging from 10^3 up to $5.4 \cdot 10^4$. A typical I-V characteristic for a 100 x 100 μm^2 $Ag/Al_2O_3/Al$ device is shown in Fig. 2 (a). This curve was measured at T = 65 mK and in zero applied magnetic field. The measured R_N is 0.19 Ω. The I-V characteristic clearly shows the appearance of a small supercurrent of approximately 350 μA. Thus instead of a pure NIS tunnel junction we have an S'IS junction. Due to the proximity effect the Ag base electrode no longer behaves as a normal metal. The Al base film underneath the Ag induces an energy gap Δ_{Ag} of 50 μeV. This effect can clearly be seen in Fig. 2 (b) where only the subgap region is shown in zero applied magnetic field at temperatures of 75, 200, 250, 300 and 425 mK. In these I-V characteristics one can clearly see the current steps at the bias voltages of 50 μV corresponding to $V_{bias} = \Delta_{Ag}/e$, 130 μV corresponding to $V_{bias} = (\Delta_{Ag} - \Delta_{Al})/e$ and 230 μV corresponding to $V_{bias} = (\Delta_{Ag} + \Delta_{Al})/e$. When the temperature is increased it can be seen that Δ_{Ag} is reduced until at T = 430 mK the Ag base electrode becomes normal. In Fig. 2 (c) we show I-V characteristics measured at T = 180 mK and at different applied magnetic fields of B = 2, 3, 3.5, 4 and 4.5 mT. We can clearly see that the Ag base electrode is driven normal by the applied magnetic field and that at B = 4.5 mT we have a pure NIS tunnel junction.

Next a $Ag/Al_2O_3/Al$ device, with a 200 x 300 μm^2 Ag base electrode and a 100 x 100 μm^2 Al counter electrode, was irradiated by a ^{55}Fe source. We did not collimate the X rays and irradiated the whole Ag base film. The source emits Mn Kα and Mn Kβ photons at 5.89 and 6.49 keV respectively. For measuring the X-ray induced current pulses we applied a magnetic field of 4.5 mT parallel to the junction barrier to suppress the small supercurrent and to operate the device as an NIS tunnel junction. The junction was voltage biased by a parallel resistance of 44 mΩ. The current tunneling through the junction was monitored using a high-bandwidth SQUID-array-based current amplifier manufactured by HYPRES Inc.

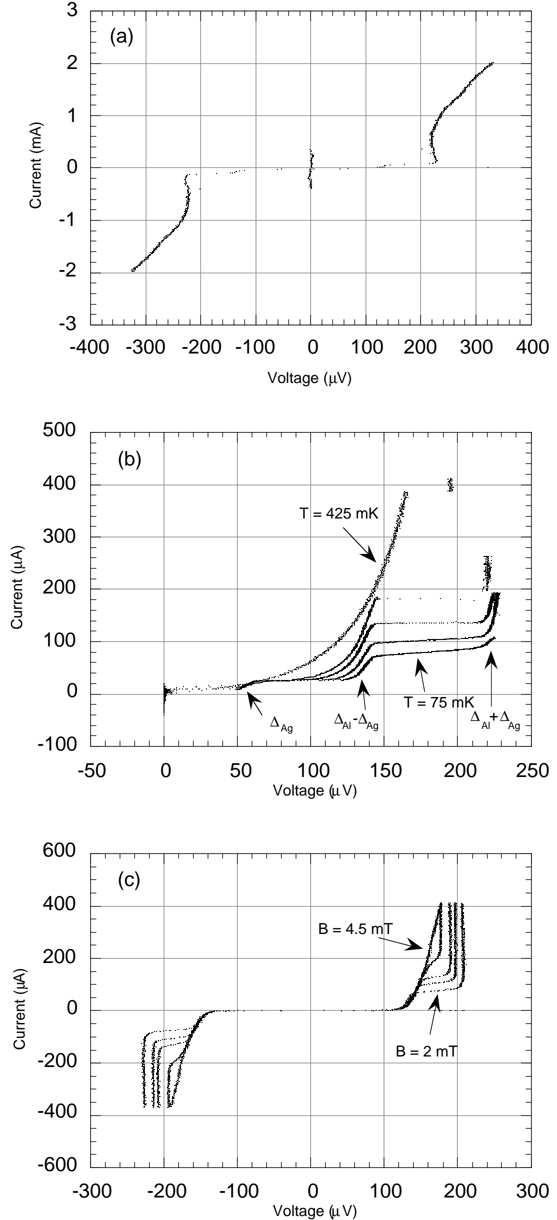

Fig. 2. Typical I-V characteristics of $Ag/Al_2O_3/Al$ tunnel junction on an Al base film. (a) Measured in zero applied magnetic field at T = 65 mK. (b) Detailed subgap measurements in zero applied magnetic field at T = 75, 200, 250, 300 and 425 mK. (c) Measured at T = 180 mK and B = 2, 3, 3.5, 4 and 4.5 mT.

[4]. We operated the amplifier in open-loop mode and its output was digitized after filtering by a 2-pole RC filter with a cut-off frequency of 5 MHz. The resulting X-ray spectrum for this device when voltage biased at 153 μV is shown in Fig. 3. The peaks due to the Mn Kα and Mn Kβ can be seen and the full width at half maximum (FWHM) energy resolution at 5.89 keV is approximately 450 eV. In Fig. 4 we show the scatter plot of the rise time versus pulse height of the 3000 current pulses. We clearly see two distinct groups with different rise times and pulse heights. These two groups are caused by absorption in the Ag base electrode either

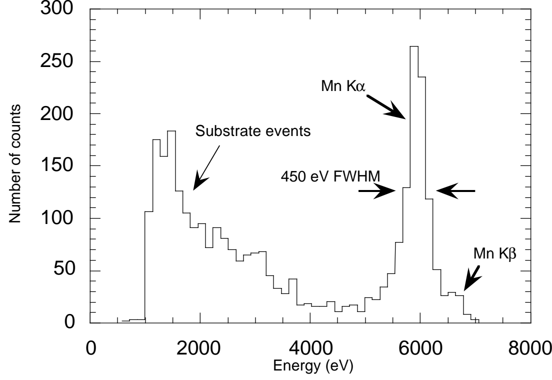

Fig. 3. Energy spectrum of a $Ag/Al_2O_3/Al$ device, with a 200 x 300 μm^2 Ag base electrode and a 100 x 100 μm^2 Al counter electrode voltage biased at V_b = 153 μV and irradiated by a ^{55}Fe source.

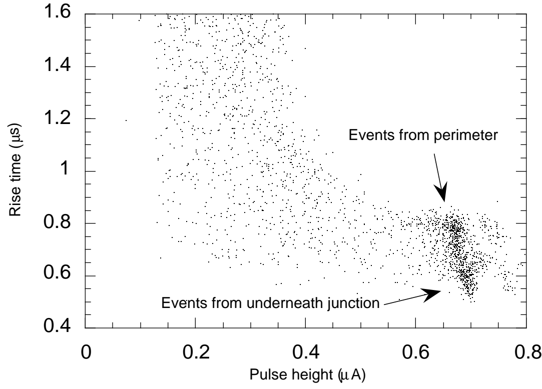

Fig. 4. Scatter plot of the rise time versus the pulse height of 3000 pulses. There are two distinct groups visible with different rise times and pulse heights.

directly underneath the junction area or in the perimeter outside the junction area. The events that are absorbed in the perimeter have slightly slower rise times and smaller pulse heights than the events absorbed directly underneath the junction area. The slower rise times are due to the time needed for the diffusion of the hot electrons through the Ag base electrode. The smaller pulse heights are due to electron-phonon scattering which takes place as the hot electrons diffuse to the tunnel region.

The difference between the average rise time of the absorption events underneath the junction and those in the perimeter was constant over a wide range of temperature and bias voltage. This suggests the difference in rise time is the average time it takes for the hot electrons to diffuse from the perimeter to the tunnel region. With a diffusion time $\tau_{diff} = \Delta\tau_{rise} = 0.14$ µs, and an average distance of 150 µm we estimate the diffusion constant in the Ag base electrode film: $D = \langle x\rangle^2/2\cdot\Delta\tau_{rise} = 0.080\ m^2/s$.

In Fig. 5 we show a spectrum obtained using only those pulses with a rise time smaller than 0.65 µs, thus including only those absorption events directly underneath the junction area and excluding those in the perimeter. The FWHM energy

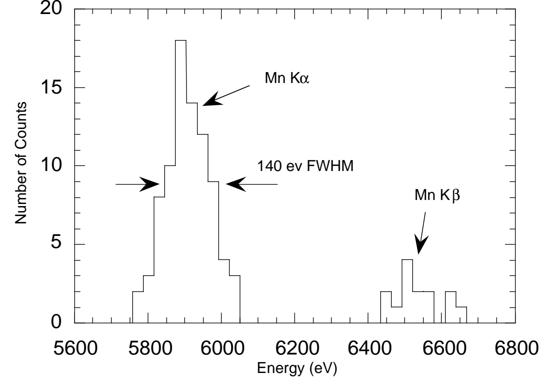

Fig. 5. Energy spectrum obtained using only those pulses from absorption events directly underneath the junction area.

resolution is now 140 eV and the Kα and Kβ lines are clearly separated.

The hot electrons that are created by an absorption of an X ray can relax back to equilibrium by electron-phonon scattering. The time the hot electrons will spend in the Ag base electrode is longer for the events absorbed in the perimeter than for events absorbed directly underneath the junction area. The additional loss factor for events in the perimeter is given by $\exp(-\tau_{diff}/\tau_{e-p})$ in which τ_{e-p} is the electron-phonon scattering time. The relative pulse-height difference between events under the junction and those in the perimeter should be determined by τ_{diff}/τ_{e-p}. From an average relative pulse-height difference of 5% we estimate $\tau_{e-p} = 2.8$ µs.

In Fig. 6 we show that the relative pulse-height difference increases with temperature, and the typical decay time τ_{decay} of the current pulses decreases with temperature. Increasing the temperature reduces the electron-phonon scattering time $\tau_{e-p} \sim T^{-n}$ [5], where n is either 4 or 5, and thus gives shorter decay times and a larger relative pulse-height difference.

Tunneling through the barrier to the Al counter electrode provides an additional relaxation mechanism for the hot electrons. Since the total relaxation rate is given by the sum of the individual rates, the decay time of the current pulse is

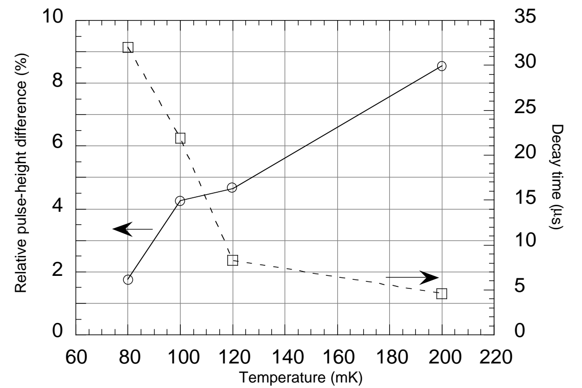

Fig. 6. Relative pulse-height difference between events absorbed underneath the junction area and those in the perimeter, and decay time as a function of temperature. All data measured at low applied bias voltages.

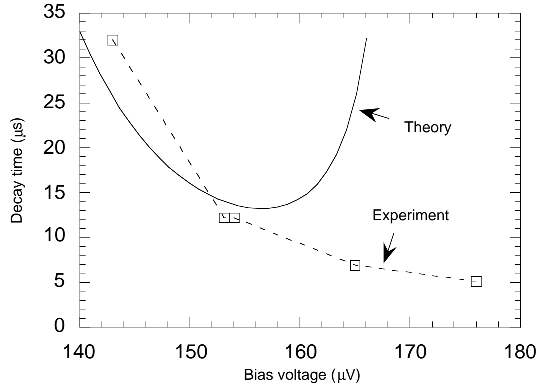

Fig. 7. Theoretical (solid line) and measured (dashed line) decay time of the current pulses as a function of applied bias voltage at constant temperature. The theoretical model predicts longer decay times for bias voltages close to Δ/e. The experimental data don't show this increase because of a reduction of the electron-phonon scattering time caused by an increase in temperature.

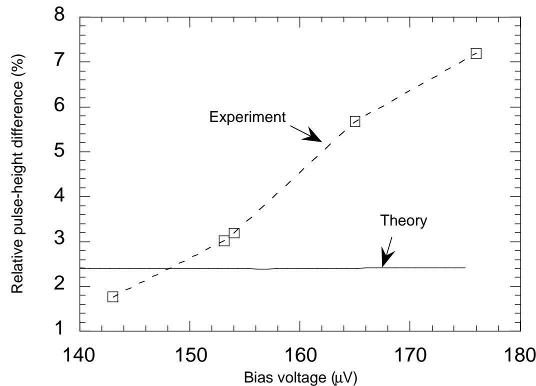

Fig. 8. Theoretical (solid line) and measured (dashed line) relative pulse-height difference as a function of applied bias voltage at constant temperature. The increase in the observed relative pulse-height difference with bias voltage suggests that hot electrons are relaxing faster due to higher junction temperatures at higher bias voltages.

given by $1/\tau_{decay} = 1/\tau_{e\text{-}p} + 1/\tau_{NIS}$. The tunneling time τ_{NIS} depends on the bias voltage V_b applied across the junction and exhibits a minimum just below $V_b = \Delta/e$. The fast tunneling at this minimum reflects the singularity in the density of states of the superconducting electrode. From this we expect a minimum in the decay time of the current pulse when measured at different bias voltages. The measured decay time, which is shown in Fig. 7, decreases with bias voltage, but does not show the expected increase at $V_b = \Delta/e$. This suggests a rise in temperature at higher bias voltages and thus a reduction of the electron-phonon scattering time $\tau_{e\text{-}p}$. The higher bias current at higher bias voltage should actually cool the normal electrode as the hottest electrons tunnel away from the normal metal. In our devices, however, the hot electrons are confined in the superconducting counter electrode, and thus return much of the heat to the normal metal electrode.

This heating effect is also indicated by the change in relative pulse-height difference as a function of the applied bias voltage, which is shown in Fig. 8. If the temperature were constant, the pulse-height difference would not change with bias voltage since the pulse-height difference hardly depends on the tunneling time τ_{NIS}. The larger pulse-height difference at high bias voltage can be explained by a temperature induced increase in electron-phonon scattering of hot electrons as they diffuse to the tunnel region.

4. Conclusions

We have used a new process to fabricate $Ag/Al_2O_3/Al$ NIS tunnel junctions onto a superconductor. We plan to use this process to fabricate high-resolution X-ray detectors using high-Z, ultra-pure superconducting crystals as absorbers. The superconductor introduces an energy gap in the normal electrode by the proximity effect. We studied the dependence of this energy gap on temperature and applied magnetic field. By using a high-bandwidth SQUID to record the current pulses, the diffusion of the hot electrons can be measured. By means of a rise time cut, it is possible to select signals only from events absorbed directly underneath the junction area. The X-ray energy resolution of these events was 140 eV FWHM at 6 keV. With a normal electrode much larger than the junction area, we could determine the diffusion constant for hot electrons in Ag and the typical electron-phonon scattering time. The measurement of the current pulse decay time and relative pulse-height difference between events absorbed under the junction and those absorbed in the perimeter, show that the normal metal heats as the bias voltage is increased. This heating can be avoided in future devices by attaching a heat sink to the superconducting electrode.

Acknowledgment

We would like to thank J. Batteux for his technical assistance in many different areas.

References

[1] H. Netel, M. Frank, S. E. Labov, G. H. Campbell, C. A. Mears, E. Brunet, L. J. Hiller and M. A. Lindeman, "Development of a prototype superconducting X-ray spectrometer using a Ta crystal as absorber," *Nucl. Instr. and Meth.* A, vol. 370, pp. 47-49 (1996).
[2] C. A. Mears, Simon E. Labov, M. Frank, M. A. Lindeman, L. J. Hiller, H. Netel and A. T. Barfknecht, "Analysis of pulse shape from a high-resolution superconducting tunnel junction X-ray spectrometer," *Nucl. Instr. and Meth.* A, vol. 370, pp. 53-56 (1996).
[3] M. Nahum and John M. Martinis, "Hot-electron microcalorimeters as high-resolution x-ray detectors," *Appl. Phys. Lett.*, vol. 66, pp. 3203-3205 (1995).

[4] R. P. Welty and J. M. Martinis, "Two stage integrated SQUID amplifier with series array output," *IEEE Trans. on Appl. Supercond.*, vol. 3, pp. 2605-2608 (1993).

[5] F. C. Wellstood, C. Urbina and John Clarke, "Hot-electron effects in metals," *Phys. Rev. B*, pp. 5942-5955 (1994).

Technical Information Department • **Lawrence Livermore National Laboratory**
University of California • Livermore, California 94551